NUCLEAR SIMULATION AND RADIATION PHYSICS INVESTIGATIONS OF THE TARGET STATION OF THE EUROPEAN SPALLATION NEUTRON SOURCE

ACCELERATORS

KEYWORDS: *particle transport codes, pulsed-neutron source, spallation*

DETLEF FILGES,* RALF-DIETER NEEF, and HARTWIG SCHAAL
Forschungszentrum Juelich GmbH, Institut fuer Kernphysik, D-52425 Juelich, Germany

Received March 3, 2000
Accepted for Publication March 9, 2000

The European Spallation Neutron Source (ESS) delivers high-intensity pulsed particle beams with 5-MW average beam power at 1.3-GeV incident proton energy. This causes sophisticated demands on material and geometry choices and a very careful optimization of the whole target system. Therefore, complex and detailed particle transport models and computer code systems have been developed and used to study the nuclear assessment of the ESS target system. The purpose here is to describe the methods of calculation mainly based on the Monte Carlo code to show the performance of the ESS target station. The interesting results of the simulations of the mercury target system are as follows: time-dependent neutron flux densities, energy deposition and heating, radioactivity and afterheat, materials damage by radiation, and high-energy source shielding. The results are discussed in great detail. The validity of codes and models, further requirements to improve the methods of calculation, and the status of running and planned experiments are given also.

I. INTRODUCTION

During the last decade several spallation neutron sources [the Intense Pulsed Neutron Source[1] (IPNS), the Spallation Neutron Source at Rutherford Appleton Laboratory[2] (ISIS), the Pulsed Spallation Neutron Facility[3] (KENS) at the High-Energy Accelerator Research Organization (KEK), the Los Alamos Neutron Scattering Center[4] (LANSCE), the Schweizerische Intensive Neutronen Quelle[5] (SINQ), and the Zero Gradient Synchrotron Intense Neutron Generator-Prototype[6] (ZING-P) at Argonne National Laboratory (ANL)] started operation. The experience of these facilities encouraged the scientific community to start new projects to develop next generation neutron sources to increase the usable neutron fluxes by at least one order of magnitude. It seems possible for the European Spallation Neutron Source[7] (ESS) project based on a proton accelerator of 5-MW beam power to reach a maximum pulsed peak thermal neutron flux of $\sim 2 \times 10^{17}$ n/(cm^2·s) in the moderator.

A 5-MW spallation neutron source engineering study was initiated in Germany as Spallations Neutronen Quelle[8] (SNQ). A first ambitious project was the proposal of a continuous spallation source at Chalk River—the Intense Neutron Generator[9] (ING)—with a Pb-Bi target, 1-GeV proton beam, and a proton current of 65 mA.

The other spallation neutron source projects are based on 1-MW proton beam power. Studies are performed at ANL (Ref. 10), Brookhaven National Laboratory[11] (BNL), KEK (Ref. 12), Los Alamos National Laboratory[13] (LANL), and Oak Ridge National Laboratory[14] (ORNL). The first 1-MW neutron spallation source already in operation is SINQ (Ref. 15), which is a continuous source.

The planned use in each of the aforementioned cases needs high-intensity particle beams, which cause sophisticated demands on reliability of materials, e.g., for containment and target. Therefore, complex and detailed particle production and transport models and computer code systems have been developed. The utilized models and codes were extensively tested and validated in connection with the existing pulsed and continuous neutron spallation sources for condensed matter studies and with detector and hadron calorimeter development at meson factories and high-energy accelerators.

II. THE MERCURY TARGET SYSTEM FOR ESS

The target system is crucial for the feasibility and performance of the whole spallation neutron source. In

*E-mail: d.filges@fz-juelich.de

existing facilities, only spallation targets with pulsed beam powers of at least a factor 30 less than envisaged for ESS have been operated. This large step in power made it prudent to choose a design for the target that has future development potential, rather than one based on existing concepts, which might approach the limits of feasibility.

By design, the ESS target will be subject to high loads from power density and thermal cycling. While these effects may be deleterious to a heterogeneously cooled solid target, a liquid-metal target remains virtually unaffected by them. Other arguments in favor of a liquid target are its large mass and hence low specific activity even after many years of service and the fact that no active decay heat removal may be required during service and maintenance periods. In view of the foregoing considerations, the ESS target group decided in June 1995 to study a liquid-metal target with mercury as target material. The need for a high atomic number for good neutron yield, the good availability, and the fact that it remains liquid at room temperature makes mercury the number one candidate for a liquid-metal spallation target.

The high thermal neutron absorption cross section of mercury is the main reason for not considering it as a target material for steady-state spallation neutron sources, which depend on a long neutron lifetime in the moderator for high-flux densities. In the case of a short pulsed source like ESS, however, some moderators are surrounded by decouplers (neutron absorbers) to prevent moderated neutrons from returning to the moderator and deteriorating the pulse shape. In this case, the high-absorption cross section of mercury may turn out to be an advantage, because it may avoid the need for the decoupler between the target and the moderator thus reducing complexity. The fact that no water is present in the beam interaction region in a liquid-metal target means that there is virtually no moderation taking place in the target volume. This results in a harder leakage spectrum.

In view of its relative advantages over the other candidate materials (highest density, lowest possible operating temperature, and no need for auxiliary heating), mercury was chosen as the preferred liquid-metal target material. The most critical part of the liquid-metal circuit is the vessel (the target shell), which contains the liquid metal in the beam interaction zone and which is exposed to the proton beam and neutron radiation.

For the target itself, a slab-type geometry was chosen. Apart from the reflecting effect of the wings for fast neutrons, this geometry also offers the advantage of allowing an elliptical cross section of the beam to be chosen, thus reducing the current density, the associated heat load, and radiation damage in the window while keeping the distance between the beam axis and the moderators small. Typical dimensions of the target in the interaction region are 14 cm (high) and 30 cm (wide), with an elliptic cross section of the beam of 6-cm vertical axis and 20-cm horizontal axis at the entry window. The front cover of the target (beam entry window) is curved in two dimensions, with a constant radius of curvature in the vertical plane and an elliptical contour in the horizontal one, in order to minimize the stress resulting from thermal gradients and internal pressure.

III. REQUIREMENTS OF CALCULATIONAL METHODS

To study and develop high-power spallation targets, we had to prepare the method of calculation and computer codes into an integrated but modular system. We began to develop the computer code system high-energy radiation Monte Carlo elaborate system[16] (HERMES) during the SNQ project[8] and updated it for our ESS studies. Details are given in Ref. 17. We have to answer the following important questions and predictions for high-current accelerators and their target stations:

1. neutron, gamma, and charged-particle production and fluxes
2. energy deposition and heating
3. radioactivity and afterheat
4. materials damage by radiation
5. high-energy source shielding.

The main goal of the calculation is the optimization of the neutron flux.

Particle fluxes and power density are mainly influenced by the possibilities of cooling the target, the window, and the containment. Temperature gradients have to be kept in certain limits to avoid failure by stress. Radiation damage is produced by different mechanisms as displacements per atom (dpa), gas production, and nuclide transmutation, which worsen the mechanical properties and limit the lifetime of the target- and structure materials. Activation leads to global hazard rating of the target station. Cooling circuits with their radiolysis and corrosion problems of light and heavy water have to be studied, especially, because radioactivity is transported through pumps, valves, and heat exchangers outside the target containment. Shielding of spallation facilities is different compared to nuclear reactor systems and fusion devices due to the high-energy neutron component that influences the safety and environment. Finally, the uncertainties of the simulations should be assessed based on comparisons of the results of calculations with benchmark experiments. The development, construction, and operating experience has been published in great detail in the ICANS I-XIII-proceedings[18] in the last 20 yr.

IV. GENERAL DESIGN CHARACTERISTICS OF THE HERMES MONTE CARLO SYSTEM

To simulate the histories, i.e., production, interaction with matter, and transport, of high energetic particles, the latest state-of-the-art radiation transport

codes and event generators are used in HERMES (Ref. 17). All the codes employ Monte Carlo techniques with three-dimensional geometry description. With HERMES, it is possible to treat in detail the reaction mechanism and the transport of the high-energy particles as well as of the low-energy particles created. All codes make use of a common data interface named the "HERMES Submission File." With this off-line coupling, it is much easier to implement additional Monte Carlo codes or to replace codes. Thus, HERMES can be extended in an easy way to represent the state of the art, without need for changing programs. Results from the models utilized may be received as intermediate results to improve the understanding of the problem and the dependency between these models.

The problems that can be solved with the aid of the HERMES system cover a wide range of incident particle energies and a set of particle types. Therefore, the computational work had to be shared between several Monte Carlo codes, each solving a specific part of the general problem. Currently, four Monte Carlo codes are implemented, namely HETC, MORSE-CG, MCNP, and EGS4 [see references in HERMES (Refs. 16 and 17)]. A description of the system, including the communication file structure and the particle and the detector data flow, is illustrated in Fig. 1.

V. EXAMPLES OF MODEL APPLICATION FOR THE TARGET STATION DURING THE ESS PROJECT

In the beginning of the ESS project, we calculated a double wheel target and a double split target with

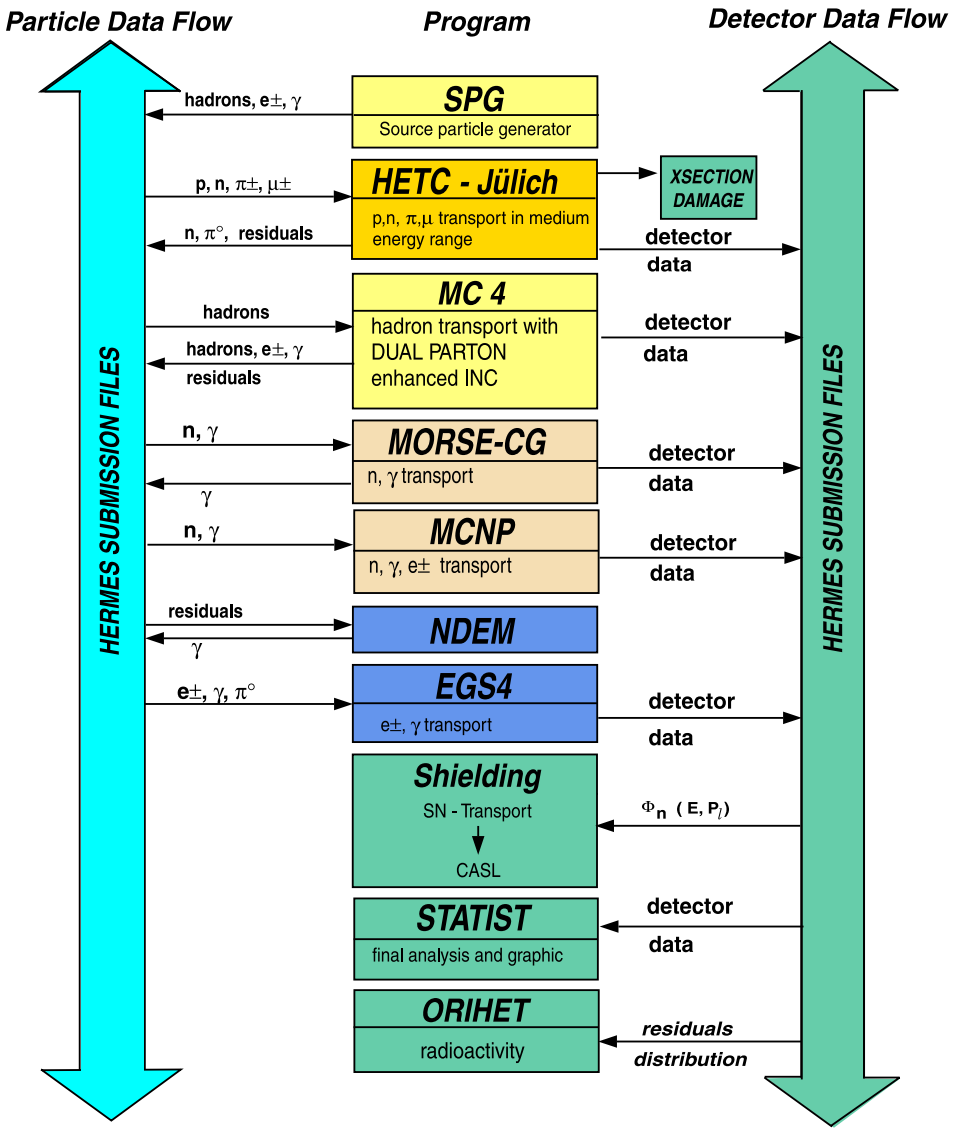

Fig. 1. Organization of the HERMES program system for theoretical studies on beam material interactions.

tungsten target plates and water cooled, with three moderator positions: the first moderator in front of the target, the second moderator in the flux trap position between targets one and two, and the third moderator behind the second target. Details of the geometry are given in Ref. 19. The incident proton energy was varied between 800 and 3000 MeV. Some examples during the course of the ESS target station development should be pointed out.

Figure 2 shows the proton-energy-dependent power deposition in the first part of the split target and in the whole target. Between 800 and 1600 MeV, there is a strong decrease of power deposition, which is much less versus higher proton energies. From this figure, the proton beam for a target should not be far below 1500 MeV.

We also investigated the power density in the target plates in a circular area of 1-cm radius around the proton beam axis. Figure 3 shows a power density of 11 kW/cm^3 in the first two target plates. This power density is reduced by a factor of 2 by increasing the proton beam energy from 800 to 1600 MeV. A further doubling of the proton energy gives less reduction than a factor of 2 for the power density.

Each proton pulse of a 5-MW accelerator at 50 Hz contains an energy of 100 kJ that is introduced into the target. This produces a space-dependent temperature jump in the target material. In Fig. 4, the temperature jump is plotted for the first tungsten target plate as a function of proton beam diameter in an area of radius $r = 1$ cm for three proton energies. We see for a Gaussian-shaped circular proton beam ($1\sigma = \pm 2.5$ cm) truncated at a 10-cm diameter a temperature jump of 40, 25, and 15 K for 800, 1600, and 3000 MeV, respectively.

VI. NEUTRON FLUX STUDIES OF TANTALUM, TUNGSTEN, AND MERCURY TARGETS

Based on the foregoing survey calculations, we compared the nuclear properties of three target material candidates, namely tantalum, tungsten, and mercury. The tantalum and tungsten targets consist of three water-cooled stacks of slightly one dimensionally bent rectangular plates. The plate configuration has the front dimension of 12×40 cm^2. The dimension increases to 16×40 cm^2, and the overall length is 69 cm. For the mercury calculation, the target material and coolant was replaced by mercury.[20] For optimal positioning of the moderators, it is important to know the distribution of the neutron flux density along the surface of the target.

Figure 5 shows that for an uncooled lead reflector, the cooled tantalum target delivers the lowest neutron current. A cooled tungsten target gives a total neutron current that is ~20% higher in the maximum. The highest total neutron current at the target surface is produced by the mercury target and is >30% higher compared to the tantalum target. Especially along the target surface, the current gradient in the case of Hg is lower than that in

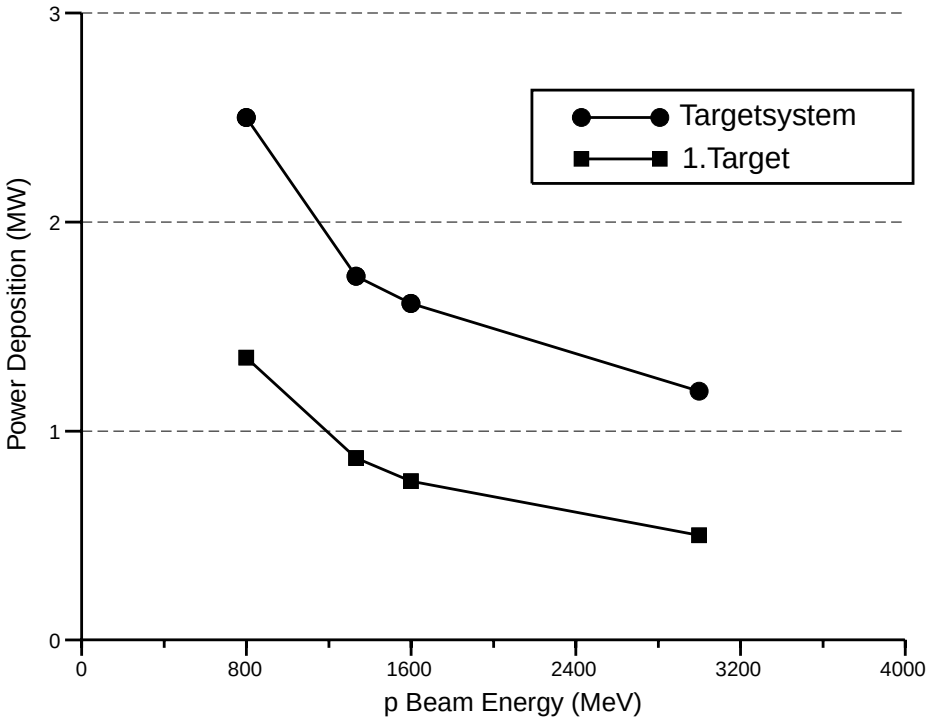

Fig. 2. Power deposition in target systems as a function of incident proton energy.

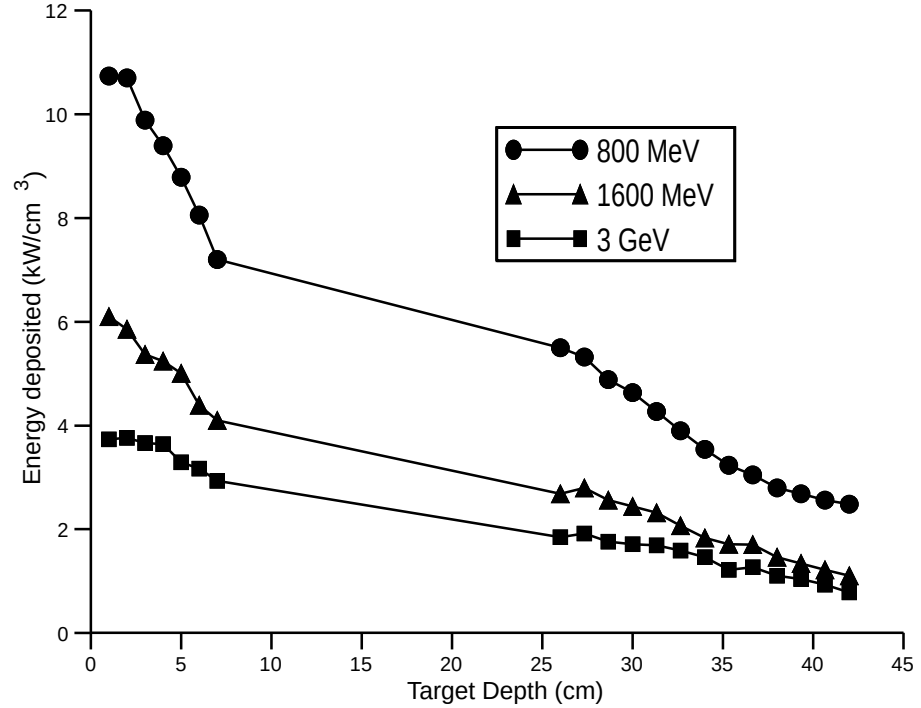

Fig. 3. Energy deposited in target plates in an area of 1-cm radius around the beam axis.

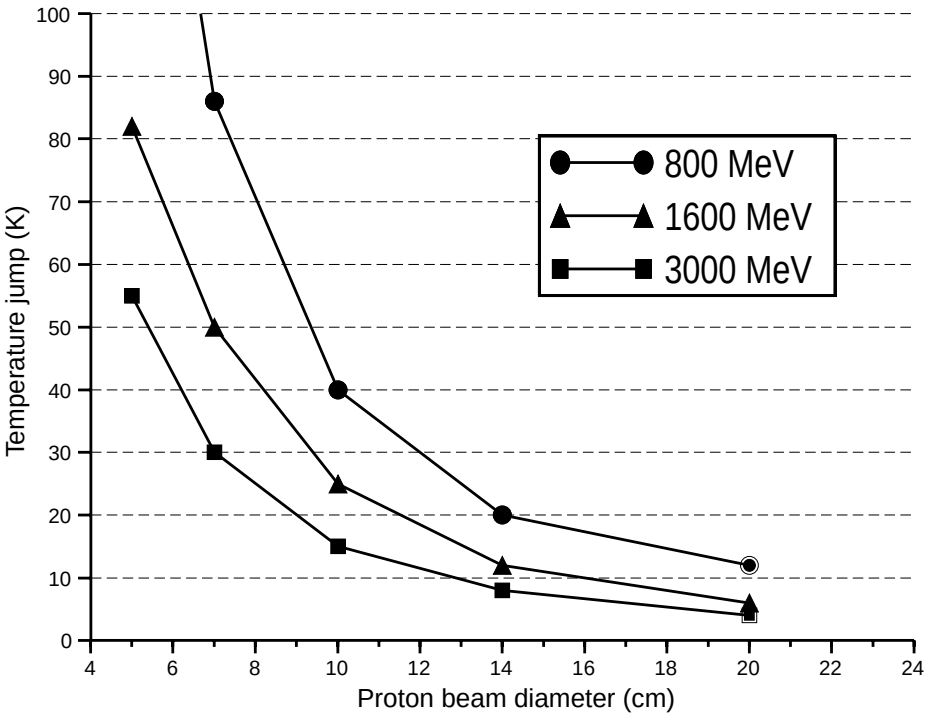

Fig. 4. Temperature jump per proton pulse in the tungsten target as a function of proton beam diameter for different beam energies around the beam axis.

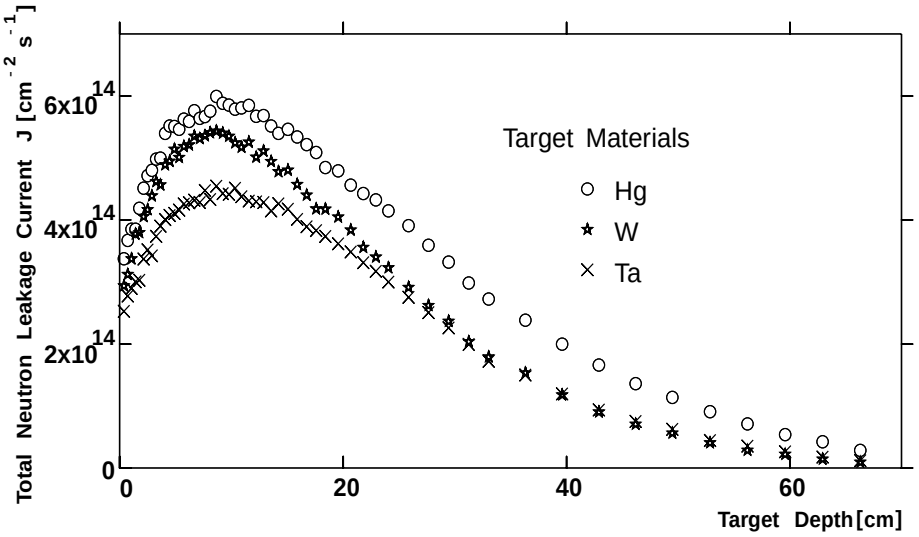

Fig. 5. Leakage distributions for neutrons <20 MeV of reflected and cooled Ta, W, and Hg targets.

the case of the W target. This means that downstream moderators receive an even higher percentage of neutrons in the case of mercury. Table I shows a comparison of possible fast and thermal neutron fluxes averaged about the moderator volume.

VII. THE PERFORMANCE OF THE ESS MERCURY TARGET STATION

VII.A. Moderator Neutron Fluxes

The ESS is a short pulsed neutron source with a proton pulse length of 1 μs and a repetition rate of 50 Hz. The goal is to reach the highest possible peak neutron flux densities for an incident proton beam of 1.334 GeV and an average current of 3.75 mA or 2.34×10^{16} protons/s. For pulsed measurements, a short decay time of the neutron pulse is also essential. Therefore, the influence of the reflector materials and coolants on pulse height and decay time has to be studied.

TABLE I

Fast and Thermal Neutron Fluxes of Ta, W, and Hg Targets

Target	Φ_{fast} [n/(cm^2·s·5 MW)]		$\Phi_{thermal}$ [n/(cm^2·s·5 MW)]	
	Upstream Moderator	Downstream Moderator	Upstream Moderator	Downstream Moderator
Tantalum	7.2×10^{13}	2.3×10^{13}	3.2×10^{14}	1.5×10^{14}
Tungsten	6.4×10^{13}	2.1×10^{13}	3.5×10^{14}	1.7×10^{14}
Mercury	8.2×10^{13}	3.5×10^{13}	3.9×10^{14}	2.3×10^{14}

The HERMES code system has been used to simulate the transport of hadrons and to estimate particle fluxes, energy deposition, and induced radioactivity. The estimations of neutron flux densities for the 5-MW target have been performed for a configuration where all four moderators were H_2O at room temperature. The detailed three-dimensional geometry configuration of the target has been considered in the simulation. Detailed descriptions are given in Ref. 7. For the Monte Carlo simulation, the following simplifications have been made (see Fig. 6):

1. The target containment consists of 5-mm-thick HT9 stainless steel.

2. Moderators are surrounded by a 13-mm-thick zone, which simulates a 3-mm-thick aluminum can and gives the possibility of adding absorber material for decoupling moderators from the reflector (e.g., 1-mm boron).

There are two moderators above and two below the target. All moderators are $120 \times 150 \times 50$ mm^3 and serve three beam channels from each visible face. The upstream ones are turned 36 deg to the proton beam axis and have axially symmetric positions. The angle between two neighboring tubes of a bundle is 12 deg. Each of the 18 neutron beam tubes has a cross section of 80×120 mm^2 (width times height).

The proton beam has a parabolic density profile with an elliptical shape of 6-cm vertical axis and 20-cm horizontal axis. The beam peak current over a pulse of 1 μs was 75 A, which is the ESS design value. All the results discussed here refer to values determined for the upstream

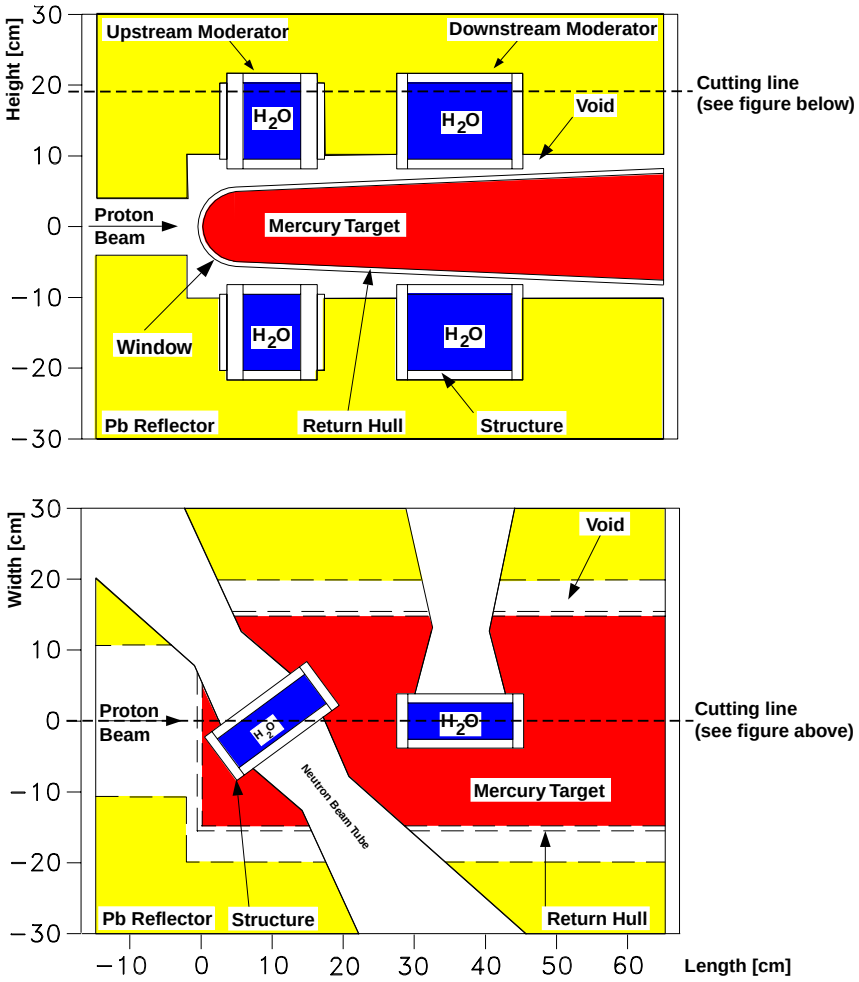

Fig. 6. Cuts through the three-dimensional target geometry for Monte Carlo simulations (outside the reflector vacuum boundary conditions are assumed; reflector size is $60 \times 60 \times 80$ cm^3), upstream moderator midpoint position is 11 cm, and downstream moderator midpoint position is 37 cm.

moderator (see Fig. 6). The time-averaged and time-dependent neutron flux densities given for the downstream moderator are ~1.5 to 2.5 times lower.

To determine average and peak neutron flux densities, the Monte Carlo calculations were based on the geometry model given in Fig. 6. The moderation time as well as the average and peak neutron flux densities are not only influenced by the moderator materials but also are highly dependent on reflector materials and geometrical arrangements. These calculations used the time-dependent Monte Carlo code MORSE-CG of the HERMES code system. HETC of HERMES uses a single, delta-shaped proton pulse to simulate the real 1-μs-long pulse containing 4.68×10^{14} protons and calculates the neutrons for MORSE.

The neutron performance of the target station is influenced by reflector size, reflector material, and moderator position, which all have to be optimized. A Be reflector of $60 \times 60 \times 100$ cm^3 gives the maximum peak neutron flux density of 1.6×10^{17} n/(cm$^2 \cdot$s), whereas a Pb reflector of $150 \times 150 \times 150$ cm^3 gives maximum peak neutron flux density of 2.1×10^{17} n/(cm$^2 \cdot$s), about 30% higher compared to the Be reflector. Also, the long-term decay constant $\tau = 165$ μs for lead is half the value of a beryllium-reflected system. The conclusion of the reflector size study is that the optimum reflector size is ~100 to 150 cm in all dimensions. For details see Table II.

Figure 7 shows the time dependence of the thermal neutron flux density in comparison for Pb- and Be-reflected uncooled systems and demonstrates the better pulse performance obtained by using a Pb-reflected target system. The optimum position of the moderators depends on the neutron leakage distribution from the target. Because of the requirement to position four moderators (see Fig. 6), there are two extremes in the optimization of the neutron flux density, either two symmetric moderators with highest possible intensity or all four moderators with equal performance. For this purpose, the

TABLE II

Expected Optimum Values of Thermal $\phi_{average}$ and ϕ_{peak} Neutron Flux Densities ($E < 0.4$ eV) of the Upstream Ambient Temperature H_2O Moderator of the ESS Mercury Target System

Reflector Material (Size)	$\phi_{average}$ (10^{14} cm$^{-2}\cdot$s^{-1})	ϕ_{peak} (10^{17} cm$^{-2}\cdot$s^{-1})	Decay Time τ (μs) ($t > 100$ μs)
Pb ($60 \times 60 \times 100$ cm^3)	4.1	1.6	132
Pb ($100 \times 100 \times 100$ cm^3)	5.4	2.0	150
Pb (15 vol% H_2O) ($100 \times 100 \times 100$ cm^3)	5.5	1.5	180
Pb (15 vol% D_2O) ($100 \times 100 \times 100$ cm^3)	6.2	1.9	150
Pb ($150 \times 150 \times 150$ cm^3)	7.1	2.1	165
Be ($60 \times 60 \times 100$ cm^3)	6.8	1.6	256
Be ($100 \times 100 \times 100$ cm^3)	7.6	1.6	290
Be (15 vol% H_2O) ($100 \times 100 \times 100$ cm^3)	6.6	1.4	245
Be (15 vol% D_2O) ($100 \times 100 \times 100$ cm^3)	7.5	1.6	260
Be ($150 \times 150 \times 150$ cm^3)	7.9	1.6	289

average thermal neutron flux density as a function of the relative position of the four moderators to the target has been determined. The results are calculated for unperturbed beryllium and lead reflectors ($100 \times 100 \times 100$ cm^3) and given in Fig. 8. These calculations give a maximum peak neutron flux density of 1.60×10^{17} n/(cm$^2\cdot$s) for the Be-reflected system with the upstream moderator midpoint positioned 11 cm downstream from the mercury-window interface (see Fig. 8). The lead-reflected system produces a peak neutron flux density of 2.1×10^{17} n/(cm$^2\cdot$s) in the upstream moderator if the midpoint is positioned at 20 cm downstream from the mercury window interface. The downstream moderator midpoint is then at 46 cm. The moderators deliver equal pulse heights of neutron pulses if the upstream moderators midpoint is positioned above/below the interface of the target window and mercury, i.e., midpoint position at ~0 cm. The midpoint distance between the upstream and downstream moderator was always fixed to 26 cm. Monte Carlo simulations, under the ideal condition that no perturbations by beam tubes are present, give the flux densities in the two moderators as shown in Table II. The influence of the coolants H_2O and D_2O are also considered, because energy deposition calculations show that the reflector system has to be cooled.

A lead-reflected mercury target system will produce the highest peak neutron flux density 2.0×10^{17} n/(cm$^2\cdot$s) and has a low, long decay time $\tau = 150$ μs, which is half the value of a Be-reflected system. Therefore, a lead-reflected mercury target is proposed. The decay constants seem to behave rather erratically when H_2O and D_2O coolant substitute for part of the reflector material.

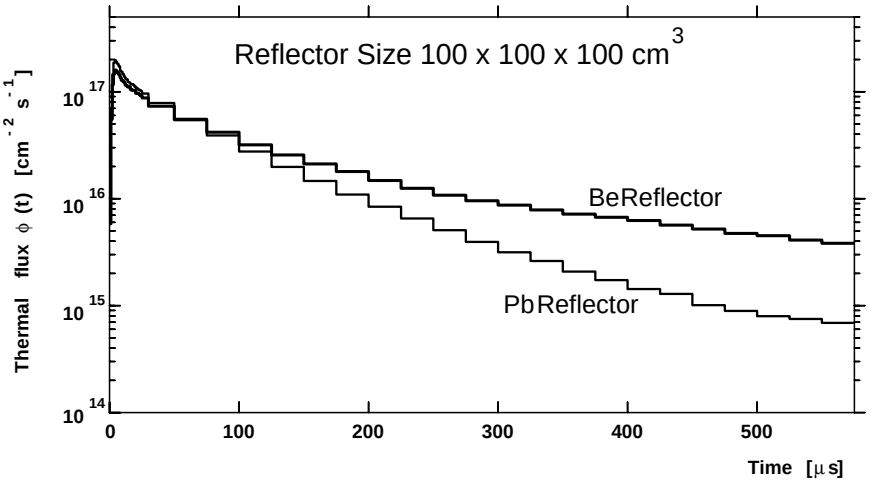

Fig. 7. Comparison of time-dependent thermal neutron flux density for Pb- and Be-reflected targets.

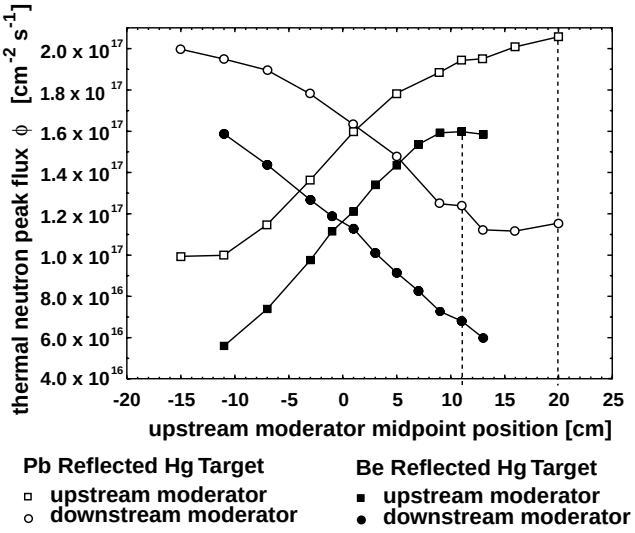

Fig. 8. Thermal peak neutron flux density as function of the relative position of moderators to the target of a Be- and Pb-reflected system with a reflector size of 100 × 100 × 100 cm^3.

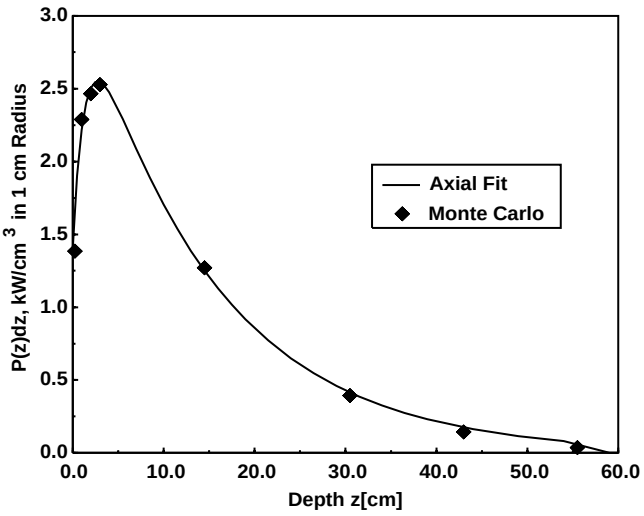

Fig. 9. Power density in the central cylinder of 1-cm radius of the mercury target for a 5-MW beam, as obtained from Monte Carlo calculations.

One has to consider that the material Pb is a pure reflector material whereas Be is also a very good moderator material, which has an important influence on the neutron spectrum. For a high-intensity upstream (front) moderator with optimum time-integrated thermal neutron flux density, the midpoint of the moderator should be at a depth of 11 or 16 cm for a Be or a Pb reflector, respectively.

The maximum thermal neutron sum flux density for all four moderators is reached when the midpoint of the upstream moderator is at −2 or 0 cm for a Be- or Pb-reflected system, respectively.

VII.B. Energy Deposition

Using the defined elliptical beam cross section, calculations for the temperature distribution in the window and the target volume were carried out. The axial distribution of the power density in the central cylinder of 1-cm radius was obtained from Monte Carlo calculations and is shown in Fig. 9 together with a fitted curve. These calculations give a total deposited power of 2372 kW, i.e., 47% of the total beam power. The rest of the beam energy is taken by escaping particles (28% in other components—e.g., reflector, shielding, and structure) and binding energy (25%).

For the power deposition in the window, Monte Carlo results yield a peak power density of 1.4 kW/cm^3 in steel, corresponding to a value of 2.27 $kW/g(mA/cm^2)$ at 79 $\mu A/cm^2$ and a density of 7.8 g/cm^3.

VII.C. Radioactivity and Afterheat

For spallation neutron sources, it is important to know the amount of radioactivity caused by beam losses in the accelerator and the beam lines. This knowledge allows one to estimate where hands-on-maintenance could be possible and where remote-handling systems should be foreseen. The calculation of the amount of radioactivity produced in the target can hint how to handle and deposit the burnt targets.

In Figure 10, the calculation procedure used in the frame of HERMES is shown. The particle production and depletion code ORIHET is developed from ORIGEN (Ref. 21). We used this procedure to compare the radioactivity and afterheat in the different materials tantalum, tungsten, and mercury proposed as target materials in the context of the ESS.

We restricted ourselves to calculate the values of the target zones only, assuming that the activity and afterheat of the surrounding reflectors, moderators, and cooling systems are nearly the same for the different target materials. The nuclide generation and depletion was calculated for a full-power ESS beam time of 1 yr and after shutdown of the beam for decay times reaching from 1 day to 100 yr. The results are given separately for those caused by spallation and those caused by neutrons with energies below 15 MeV.

The most interesting time with respect to problems of cooling and handling of the target is the shutdown time. In Table III it can be seen that the activity and thermal power caused by spallation are nearly the same for all three targets, but the amounts caused by the low-energy neutrons are quite different. The total amount of activity and afterheat is largest in the tantalum target; the mercury target shows the lowest values.

The next question is about the long-term radioactivity and afterheat production with respect to storage and waste management. The time behavior of the three targets

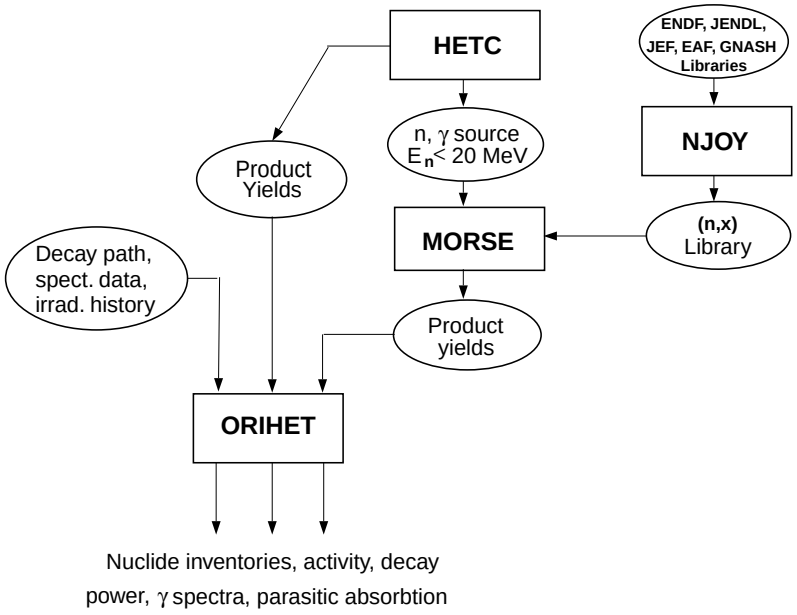

Fig. 10. Simulation procedure to calculate radioactivity and afterheat with the HERMES code system.

is shown in Figs. 11 and 12. In Table IV, for the time 100 yr after shutdown, the total values are shown that are caused by the spallation products only.

VII.D. Material Damage by Radiation

For high-power spallation targets, an essential point is the estimation of the lifetime of heavily irradiated components. Material failure has safety and economic aspects. Accelerated protons as well as produced secondary particles cause material damages mainly by three different mechanisms, such as helium embrittlement, displacements, and transmutation. Therefore, first of all, beam windows, target containment, inner target structure, and thick solid target material damages have to be studied. In the past, most research work has been performed in fusion and reactor technology for particle energies $<$20 MeV. This knowledge is very valuable, but even more important is the damage induced by particles of energies $>$20 MeV. Until now, no correct description of the experimental data on helium production and recoil energy distributions at these higher energies has yet been achieved. The procedure we used for ESS is shown in

TABLE III

Comparison of Radioactivity and Thermal Power at Shutdown Time for Different Targets for 5-MW Proton Beam Power and 1-yr Full-Power Operation

	Tantalum	Tungsten	Mercury
Radioactivity (TBq)			
Total	4.6×10^5	1.7×10^5	1.2×10^5
Caused by spallation	7.6×10^4	8.5×10^4	8.0×10^4
Caused by neutrons below 15 MeV	3.8×10^5	8.7×10^4	3.7×10^4
Thermal power (kW)			
Total power	58.0	14.0	10.0
Caused by spallation	9.8	7.6	7.9
Caused by neutrons below 15 MeV	48.0	6.6	2.0

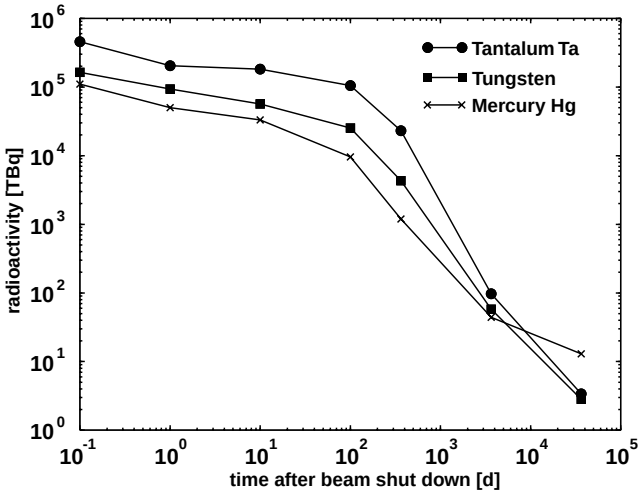

Fig. 11. Time behavior of radioactivity in terabecquerels in Ta-, W-, and Hg-targets after 1-yr full-power operation.

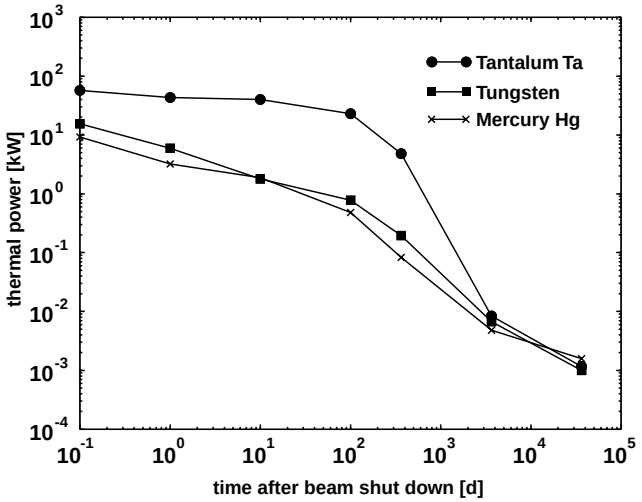

Fig. 12. Time behavior of thermal power in kilowatts in Ta-, W-, and Hg- targets after 1-yr full-power operation.

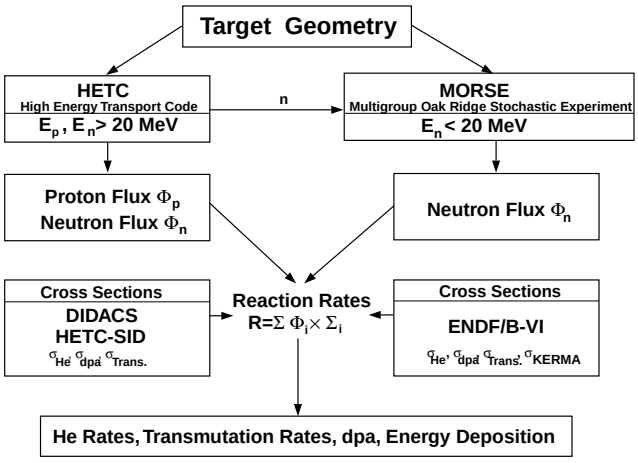

Fig. 13. HERMES method to calculate radiation damage of materials.

Fig. 13. On the other hand, the results of calculations with different models do not agree. For example, helium production is either overestimated or underestimated.[22]

Assuming a peak density of the elliptical proton beam of 80 μA/cm^2, maximum values of the damage parameters, i.e., the production, displacement, transmutation, and energy deposition, for a stainless steel (HT-9) window are given in Table V for the ESS mercury target window.

Reliable lifetime estimates are not yet possible at present. Only a lower limit based on information from a spent ISIS tantalum target and four beam windows irradiated in the Los Alamos Meson Physics Facility can be given. The ISIS target operated for several years with varying beam power and duty times that add up to an equivalent full-power service of ~1 yr. If scaled by the peak current density (80 μA/cm^2 at ESS versus 10 μA/cm^2 at ISIS), this corresponds to ~6 weeks for ESS. A comparison is shown in Fig. 14. Allowing for the fact that higher stress levels and thermal cycles may affect the lifetime, this implies a lifetime of ~6 weeks for a tantalum target at ESS. Although this is relatively short, it is the same order of magnitude as the operating time of a core in a modern high-flux reactor such as at the Institute Laue Langevin.

The doses of 10^{23} protons that steel windows survived at LAMPF are significantly higher, and these windows were routinely removed from the beam without visible damage or failure. Optimistically, one may, therefore, expect that the lifetime of a target shell will be at least two to three times longer than that of a tantalum target.

VII.E. High-Energy Neutron Source Shielding

For high-intensity spallation sources like the ESS, it is important to have properly designed shielding for the accelerator, the proton beam lines, the accumulator rings, and the target station. Overdesigned shielding would cause immense extra costs; underdesigned shielding would lead to the reduction of maximum intensity and therefore to loss of efficiency of the facility.

TABLE IV

Comparison of Total Radioactivity and Total Thermal Power After 100-yr Decay Time for Different Targets for 5-MW Proton Beam Power and 1-yr Full-Power Operation

	Tantalum	Tungsten	Mercury
Total radioactivity (TBq)	3.7	3.1	14.0
Total thermal power (kW)	1.3×10^{-3}	1.1×10^{-3}	1.8×10^{-3}

TABLE V

Maximum Damage Parameters for an HT-9 Stainless Steel Window

Maximum of the Target Window (HT-9)				
	He production (ppm/day)	Transmutation (ppm/day)	Displacement (dpa/day)	Power deposition (W/cm^3)
HETC	31.00	43.38	0.18	1326
MORSE	0.40	5.37	0.14	5
Total	31.40	48.85	0.32	1331

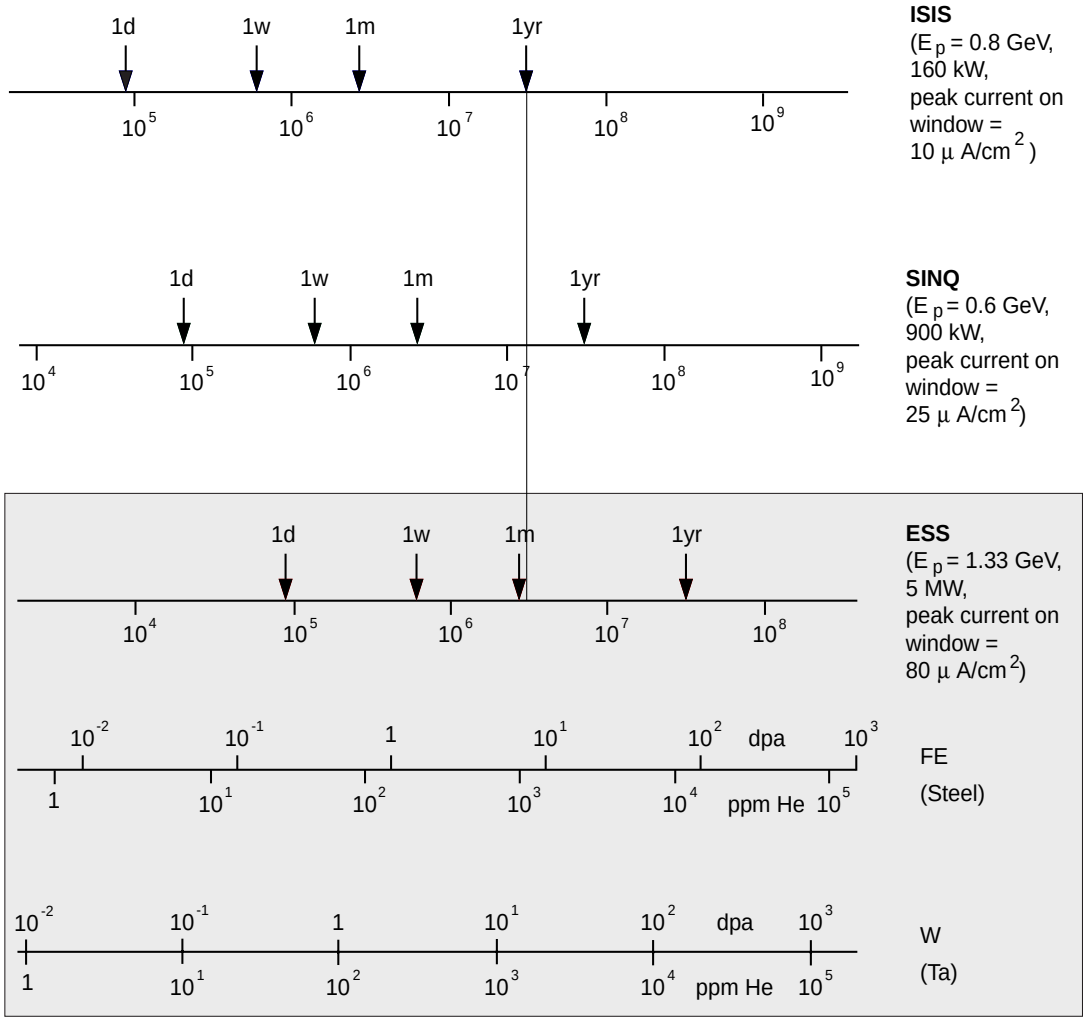

Fig. 14. Displacement and helium production in Fe and W, respectively (bottom lines), as a function of service time for targets exposed to the proton beams of ISIS, SINQ, and ESS (top lines). For comparison, a rectangular beam profile with a 7-cm diameter has been assumed in all cases, giving dpa and helium numbers averaged over the beam cross sections (Ref. 7).

The particles that cause the radiation problems are the deep-penetrating neutrons with energies >100 MeV. They determine the dose rate at each point inside the shield because they produce there via cascade a neutron spectrum with energies down to thermal energies, which is for deep penetration more or less an equilibrium spectrum if the material is not changed. Therefore, it is clear that the target station shield should consist of materials with short attenuation lengths for high-energy neutrons, whereas the shielding of tunnels etc. might consist of cheaper materials, e.g., concrete or soil.

To calculate the thickness of the shields, it seems to be reasonable to use deterministic methods instead of Monte Carlo codes because deep penetration problems lead to very high computation time to get sufficient statistics. We chose for the deep penetration two calculational methods. One is a combination of Monte Carlo codes to calculate the flux in the vicinity of the target with neutron transport codes to calculate the flux inside the bulk shield. For this coupling procedure, we use the Monte Carlo code HETC of the HERMES code system and the one-dimensional deterministic ANISN code.[23] The second method is a semiempirical one, where the geometry can be described exactly and the neutron flux and dose values are derived from integral parameters using exponential attenuation relations. The code with these features is called the CASL code.[24,25] For both methods, neutron transport cross sections are necessary, which were available only up to 800 MeV (Refs. 26 and 27), so the cross-section LAHI library[28] had to be upgraded. This was done for the energy range from 800 to 2800 MeV (Ref. 29) using the HETC code. The energy-dependent flux-to-dose conversion factors were taken from Ref. 30.

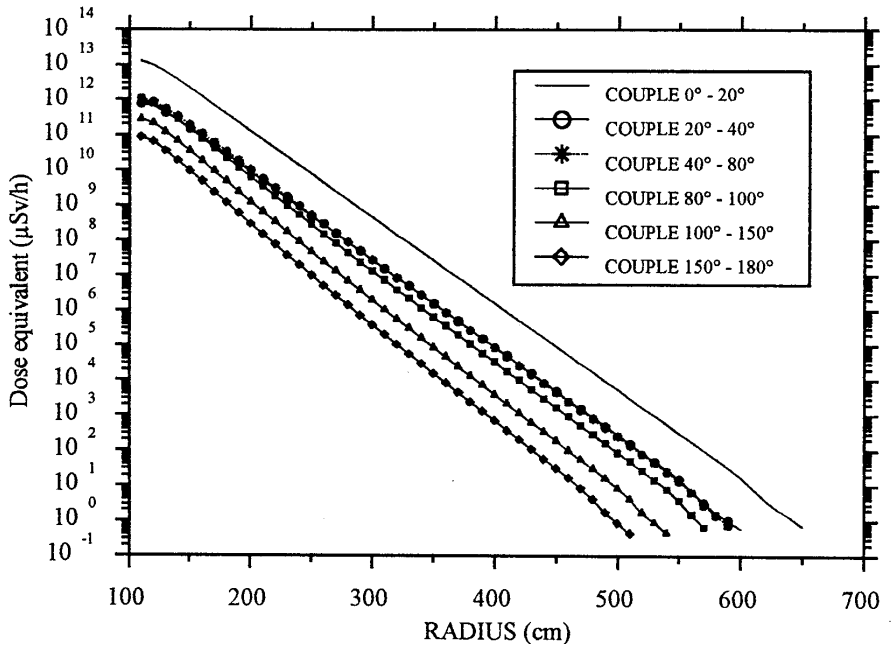

Fig. 15. Dose rates for all angular intervals versus radius of the shielding sphere.

We used the coupling procedure to calculate the dose rate behavior inside the shield for different polar angle regimes related to the proton beam direction. From Fig. 15, it can be seen that with increasing polar angle, i.e., from the forward to the backward direction, the dose rate is decreasing for the same distance from the target. Using these calculation results, we designed for the ESS a target station shield consisting of an iron cylinder with a 9-m height and a 5.2-m radius. Inside this shielding block, the target moderator reflector area is ~1 m in all directions at such a position that in the forward direction 5.2 m, in directions perpendicular to the proton beam 4.8 m, and in the backward direction 4.2 m of iron form the main target station shield. The iron shield itself is surrounded by 40 cm of concrete and based on a 3-m-thick concrete layer. As can be seen from Fig. 16, the CASL dose rate calculations show that the requirement to get a dose rate $<7.5\ \mu$Sv/h outside the shield is fulfilled.

VIII. MODEL VALIDATIONS AND FURTHER NEEDS FOR SPALLATION-RELATED DATA AND EXPERIMENTS

Many experiments have been performed to prove and validate the physical models of secondary-particle production and transport of particles through matter and their Monte Carlo simulations. Two kinds of experiments have to be distinguished—the so-called "thin" and "thick" target experiments. Cross-section measurements of double-differential particle production and excitation functions are necessary to validate the basic nuclear model assumptions. Details and results of these experiments are given in Ref. 31. As an example for double differential cross-section measurements, Fig. 17 shows the comparison of

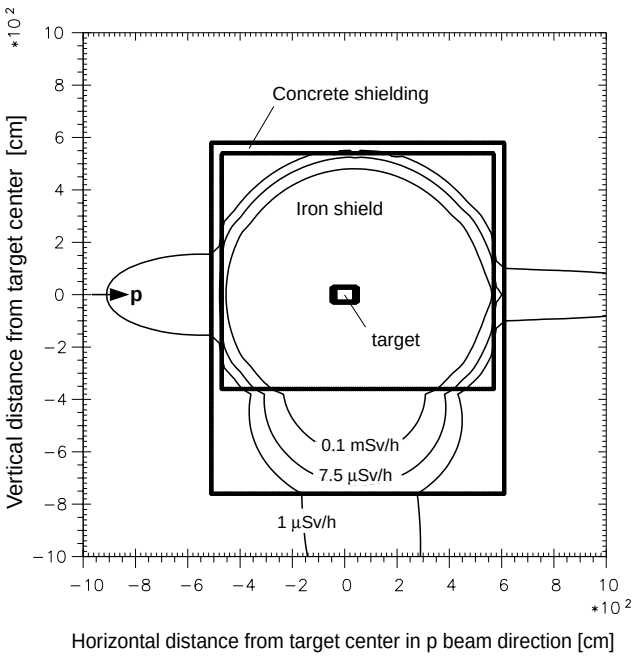

Fig. 16. Isodose rates in a vertical cross section through target shielding along the proton beam.

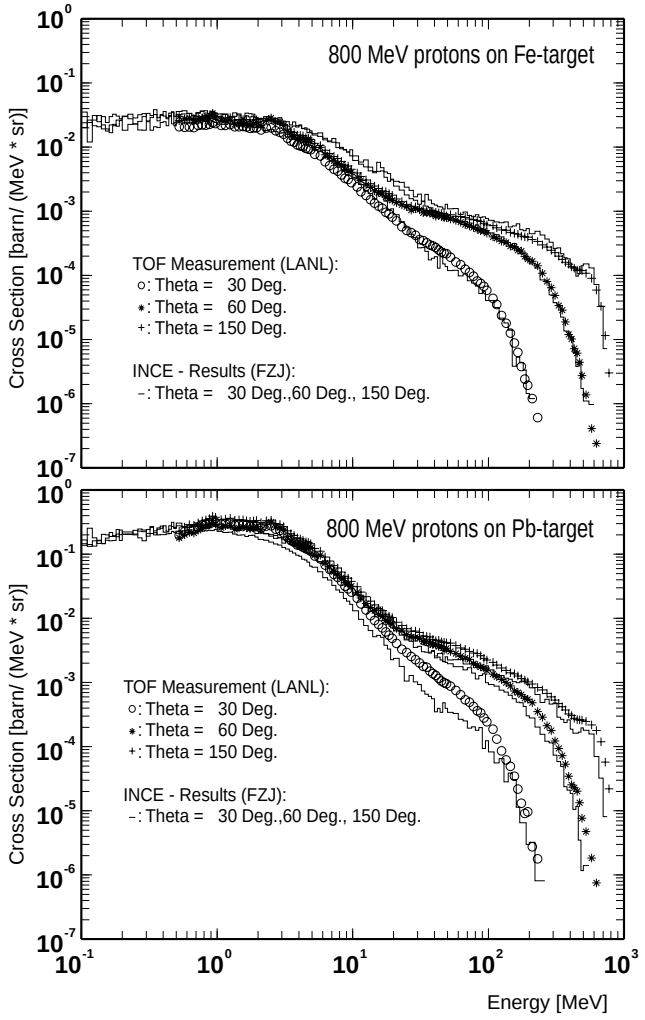

Fig. 17. Measured double-differential neutron production cross section of iron and lead and comparison with Monte Carlo calculations.

measurements and Monte Carlo calculations of the iron and lead target neutron production induced by 800-MeV protons.

The most extensive measurements are undertaken at LANL (Ref. 32) but only below 800-MeV incident proton energy. Results of measurements for higher energies have recently been published, and others are planned.[33–35] Michel et al.[36] have published a large amount of measured excitation functions of residual nuclei, which are useful to validate residual nuclei production. The knowledge of these cross sections is important for isotope production and transmutation.

A key factor in the design of each spallation target system is the neutron production in thick target systems to benchmark the code systems. In the past, many thick target experiments were performed in connection with the development of spallation neutron sources for neutron-scattering applications. These experiments included the measurements of quantities with both integral and differential natures. The most important of these was the accurate determination of the total neutron yield.[37,38] Recently new preliminary results were published and show excellent agreement for n/p ratios of lead and lithium targets except for thorium-lithium-fluoride targets with the Los Alamos code system (LCS) calculations.[39] Results of the comparison of experiments and calculations of n/p ratios are given in Table VI. A good review about results and uncertainties between different experimental groups is given in Ref. 40.

Further experiments at higher incident proton energies on "thin" and "thick" targets are planned and performed at SATURNE (Refs. 35 and 41), at CERN (Ref. 42), and at COSY-Juelich.[43] Also, high-energy calorimeter detector resolution measurements are very suitable to validate Monte Carlo simulation code systems, because one may check particle correlations and conservation laws for the shower propagation in thick targets.[44,45]

The ability to predict, on a theoretical or computational basis, all aspects of radiation physics is crucial not only to the performance optimization of the whole system but also for advising engineers in their decisions with respect to the effect on the source characteristics. While the standard of computational models for charged particle-, neutron-, and photon calculations is generally quite high, there are still some areas where more research is urgently needed. These include the following:

1. verification of cross-section and nuclear models used for mercury
2. verification of calculated integral and differential neutron flux density, secondary particle distribution, and energy deposition
3. residual nuclei distributions for induced radioactivity, afterheat, and transmutation atom generation in target and structural materials
4. correlation effects by gas production (H and He) and by recoiling nuclei in radiation damage
5. efficiency of shielding (materials combinations) against different types of radiation
6. development of scattering kernels for cold sources.

TABLE VI

Measured Neutron/Proton Ratios Compared to LCS-System Simulations

Target	Energy (MeV)	n/p Measured	n/p Calculated	Ratio Measured/ Calculated
Lead	800	22.5 ± 1.1	22.2	1.01
Th-Li-F	800	11.1 ± 0.6	12.6	0.88
Lithium	400	4.4 ± 0.3	4.4	1.00

For this purpose and the various aspects, four collaborations were organized: the Neutron Scintillator Silicon Detector (NESSI), the AGS Spallation Target Experiment (ASTE), the Juelich Experimental Spallation Target Setup in COSY Area (JESSICA), and RECOIL. Two experiments—NESSI and ASTE—are installed, and they have already delivered first results.[46]

VIII.A. The NESSI Experiment

Within the NESSI collaboration at COSY-Juelich (Cooler Synchrotron), neutron and charged-particle multiplicities are measured up to 2.5-GeV incident proton energy for thin and thick targets for various structure and target materials from Al to Pb (and U). For thin targets (only one nuclear interaction in the target), the number of evaporative neutrons is a good measure of the distribution of the thermal excitation energy induced in the nucleus. In this sense, the neutron multiplicity distribution is a sensitive test of the primary spallation process, i.e., the intranuclear-cascade part of the theoretical model. At high-excitation energies above ~2 to 3 MeV/nucleon in heavy nuclei, additional information on light charged particles improves the excitation energy resolution by approximately a factor of 2 to 3. For thick targets (multiple reactions), the alteration of the neutron multiplicity distribution reflects the production of additional neutrons produced in secondary reactions, and thus it is a sensitive test to both the intra- and internuclear-cascade part of the theoretical models.

In summary, one can show the advantage of measuring the whole neutron multiplicity distributions instead of single average values. This brings much more constraint to the intranuclear-cascade-evaporation (INCE) model. Also the measurements in both thin and thick targets appear quite complementary since, in thick targets, compensation effects between the first reaction and secondary reactions can mask deficiencies in reproducing the primary reaction by the INCE model. The thick target measurement brings an additional, although indirect, test of the thin target measurement insofar as it allows one to follow the fate of the products of the primary interaction in generating extra neutrons.

For comparison with the experiment, the simulated result with HETC-HERMES of the neutron multiplicity of a thin mercury target setup is shown in Fig. 18.

Measured and simulated neutron multiplicities are distributed very differently. Whereas the experimental multiplicity shows its maximum at 15 neutrons, the simulation shows the maximum at 23 neutrons. The detector system has an energy-dependent detection efficiency that has to be taken into account. Therefore, we have to fold the simulated neutrons with this energy-dependent detector efficiency. Then, we receive a simulated neutron multiplicity distribution that should be comparable to the measured distribution. In fact, we find a simulated distribution that tends to have a higher multiplicity by one neutron at both sides of the maximum. It is not possible to evaluate the real neutron multiplicity by experiment only, not even with the knowledge of the energy-dependent detector efficiency, because the energy of the neutrons is not measured. Therefore, the simulation is absolutely necessary for the interpretation of the experiment.

For thick targets (multiple reactions), the alteration of the neutron multiplicity distribution reflects the production of additional neutrons produced in secondary reactions, and thus it is a sensitive test to both the intra- and internuclear-cascade part of theoretical models. We have prepared target blocks (15 cm in diameter and 40 cm in length) from three materials; i.e., tungsten, mercury, and lead, which are all suited for spallation neutron sources, with Hg being favored for the ESS. These blocks are highly segmented in length and diameter, so that the neutron production at some selected proton energies can be simultaneously studied as a function of target geometry, thereby adding constraints also to the transport part of the models. The idea is to provide benchmark data for the high-energy transport codes.

In Fig. 19, a comparison of INCE and low-energy neutron transport calculations with first experimental results for thick mercury targets are given. The open triangles represent the calculated values. The stars represent calculated values folded with the energy-dependent detector efficiency to compare with the experimental results.

VIII.B. The ASTE Experiment

The purpose of the ASTE collaboration is to perform experiments to verify a number of predictions from theoretical calculations on the neutron and thermomechanical behavior of spallation targets designed for pulsed operation in the megawatt power regime. The experiments started in 1997 with a first test run with a bare cylindrical (20-cm diameter and 130-cm length) mercury target and will continue with reflected target systems.

In the experiments, the following are measured:

1. distribution of neutron leakage reaction rates
2. energy deposition distribution from 1.5- to 24-GeV incident proton beam energy
3. pressure waves in mercury
4. stress wave monitoring of the target container
5. spallation product measurements
6. reaction rate distributions in reflected target systems
7. neutron spectra by time of flight.

Of major interest in the experiment is the measurement of energy deposition distribution in the target. A pulse with all protons of the Alternating Gradient Synchroton (BNL) in two bunches, i.e., $2 \times 4.0 \times 10^{12}$ protons of 24 GeV in less than ~30 ms, introduced a

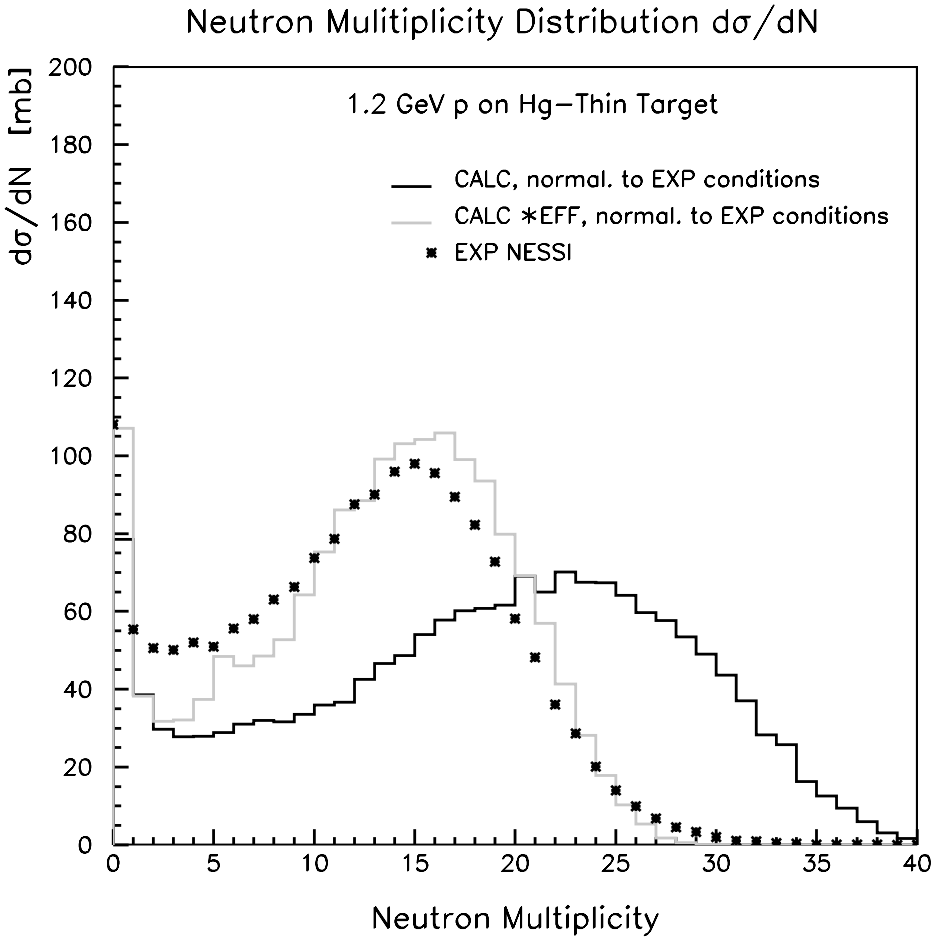

Fig. 18. Measured and simulated neutron multiplicity for 1.2-GeV protons on a thin mercury target.

maximum temperature jump of 3.4 K in the target. A comparison of the axial distribution of measured and simulated temperature jump is given in Fig. 20. The calculation was performed using the measured incident proton beam density profile.

A first comparison of calculated and measured temperature jump distribution indicates that the calculations are in good agreement with the measurements. Two further experiments are in preparation at COSY-Jülich.

VIII.C. The JESSICA Experiment

JESSICA is planned as an ESS target-moderator-reflector station mockup with in-axial-direction movable ESS mercury target. The experiments will be performed with bare and reflected target systems including beam tubes, and cooling systems for reflector and moderators. Reflector and moderator materials and geometry can be changed easily for comparable measurements. This mockup will be an advanced cold moderator test facility for ESS.

VIII.D. The RECOIL Experiment

The recently formed RECOIL collaboration (France-Germany-Poland-Russia) will study the various aspects of proton-induced reactions with nuclei by spallation physics experiments. The main part of the experimental installation is the large magnet called TETHYS from CERN with field strength of 1.2 T and wide gap of $1.0 \times 1.0 \times 0.4$ m^3 with a very homogeneous electromagnetic field. The planned experimental program consists of the measurement of spallation cross sections of recoiling nuclei over a proton energy range of 0.1 to 2.5 GeV on different target materials and also of charged particle spectra from 50 MeV to beam energy. The energy spectra of the recoiling nuclei are important to evaluate damage energy cross sections. The high-energy charged particle spectra are important to validate the distribution of the excitation energy E^*, which is the transition energy from the intranuclear cascade to the evaporation phase of the de-exciting residual nucleus.

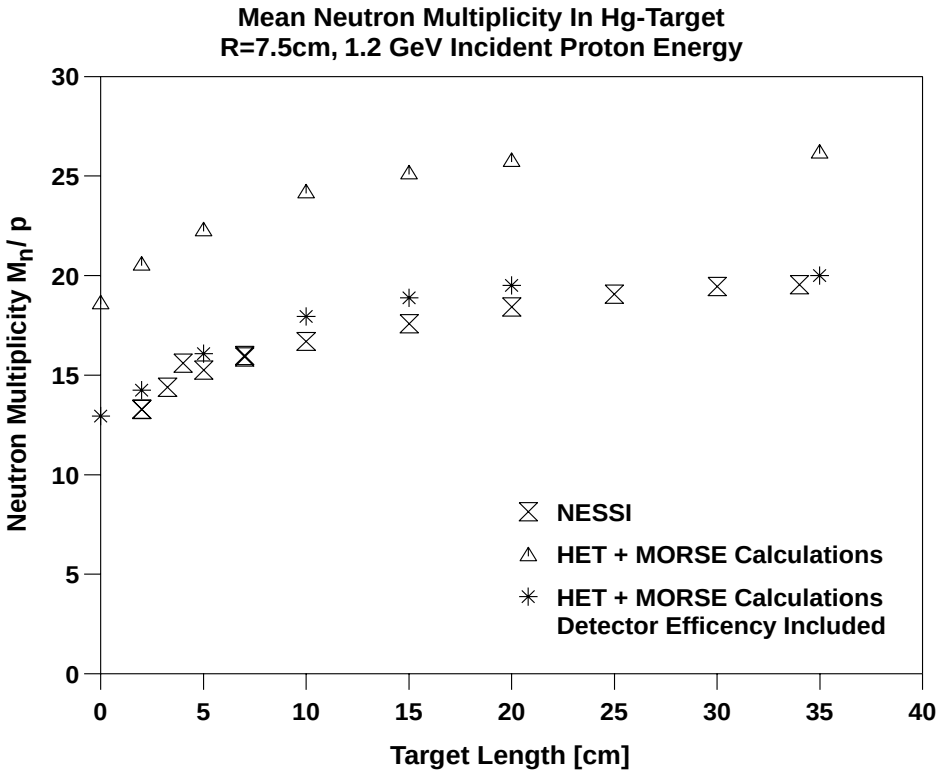

Fig. 19. Mean neutron multiplicity for 1.2-GeV incident protons on thick 15-cm-diam mercury targets.

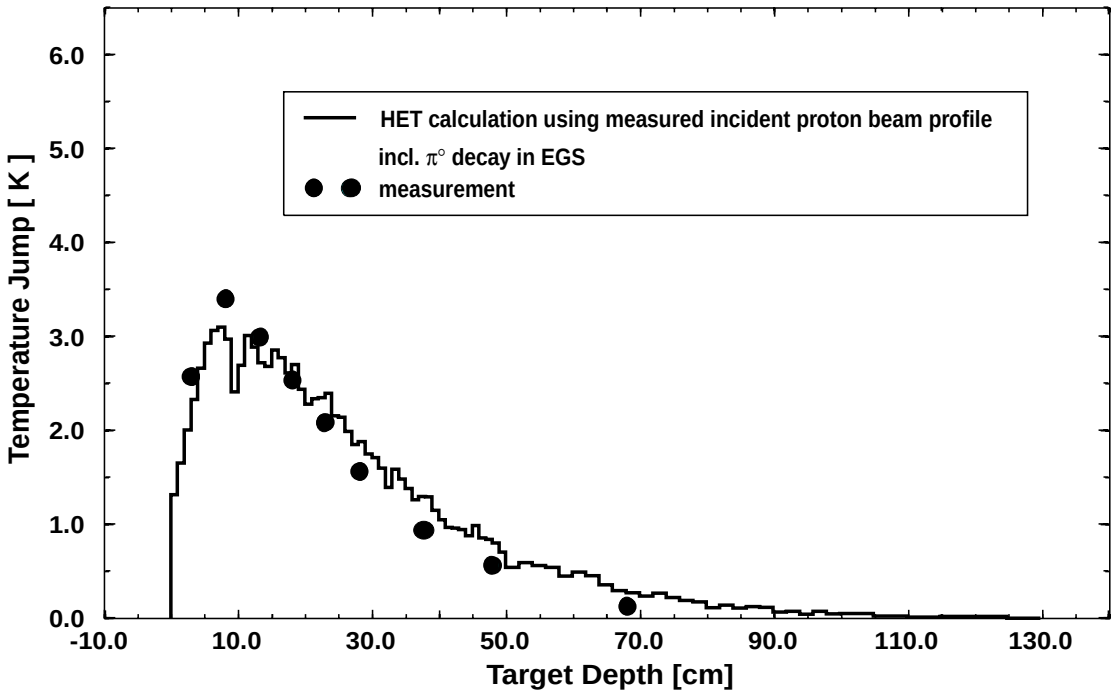

Fig. 20. Measured and calculated temperature jump in the mercury target during a 30-kJ incident proton pulse.

IX. CONCLUSION

To develop high-power spallation targets like that of the ESS, the methods of calculation have to be applied to demonstrate feasibility, to optimize the design configuration, and to support the engineering layout. The requirements of these methods in spallation technology are predictions, which have to be answered for all high-current accelerators and their target stations. The ability to predict radiation physics parameters on a theoretical basis is a crucial point for the performance optimization of the whole system by advising engineers in their decision with respect to the source characteristics. While the state-of-the-art of models and codes in applied radiation physics and particle transport is quite high, there are still some areas where more research is needed, e.g., charged particle and recoil spectra production for material damage and advanced cold moderator studies and development.

REFERENCES

1. B. S. BROWN, "News from IPNS: ICANS-XIII," *Proc. 13th Mtg. Int. Collaboration Advanced Neutron Sources*, PSI-Proc. 95-02, Paul Scherrer Institute (Nov. 1995).

2. A. D. TAYLOR, "ISIS: The First 10 Years: ICANS-XIII," *Proc. 13th Mtg. Int. Collaboration Advanced Neutron Sources*, PSI-Proc. 95-02, Paul Scherrer Institute (Nov. 1995).

3. H. IKEDA, "News from KENS: ICANS-XIII," *Proc. 13th Mtg. Int. Collaboration Advanced Neutron Sources*, PSI-Proc. 95-02, Paul Scherrer Institute (Nov. 1995).

4. R. PYNN, "LANSCE '90: The Manual Myon Jr. Neutron Scattering Center, ICANS-XI," *Proc. 11th Mtg. Int. Collaboration Advanced Neutron Sources*, KEK 90-25, National Laboratory for High Energy Physics, Japan (Mar. 1991).

5. G. S. BAUER, "SINQ as of 1998 (Status Report), ICANS-XIV," *Proc. 14th Mtg. Int. Collaboration Advanced Neutron Sources*, ANL-98/33, Argonne National Laboratory (June 1998).

6. J. M. CARPENTER, *Nucl. Instrum. Methods*, **145**, 91 (1977).

7. "The European Spallation Source Study," Vol. III, ESS-96-53-M, European Spallation Neutron Source (Nov. 1996).

8. "Realisierungsstudie SNQ," Juel-Spez-113, KfK 3175, G. S. BAUER et al., eds., Kernforschungsanlage Juelich (June 1981).

9. G. A. BARTHOLOMEV and P. R. TUNNICLIFFE, AECL-2600, Atomic Energy of Canada Limited (July 1966).

10. J. M. CARPENTER, "ICANS-XIII," *Proc. 13th Mtg. Int. Collaboration Advanced Neutron Sources*, PSI-Proc. 95-02, p. 777, Paul Scherrer Institute (1995); see also ANL-95/13, Argonne National Laboratory (1995).

11. Y. Y. LEE et al., "ICANS-XIII," *Proc. 13th Mtg. Int. Collaboration Advanced Neutron Sources*, PSI-Proc. 95-02, p. 802, Paul Scherrer Institute (1995); see also H. LUDEWIG et al., "ICANS-XIII," PSI-Proc. 95-02, p. 808, Paul Scherrer Institute (1995).

12. M. FURUSAKA et al., "ICANS-XIII," *Proc. 13th Mtg. Int. Collaboration Advanced Neutron Sources*, PSI-Proc. 95-02, p. 836, Paul Scherrer Institute (1995).

13. N. BULTMANN et al., LA-UR-95-4300, Los Alamos National Laboratory (1995); see also R. PYNN and D. WEINACHT, "ICANS-XIII," *Proc. 13th Mtg. Int. Collaboration Advanced Neutron Sources*, PSI-Proc. 95-02, p. 798, Paul Scherrer Institute (1995).

14. B. APPLETON, "ICANS-XIII," *Proc. 13th Mtg. Int. Collaboration Advanced Neutron Sources*, PSI-Proc. 95-02, p. 814, Paul Scherrer Institute (1995).

15. G. S. BAUER, TECDOC-836, p. 97, International Atomic Energy Agency (1995).

16. P. CLOTH et al., JUEL-2203, Kernforschungsanlage Juelich (1988).

17. G. STERZENBACH, P. CLOTH, D. FILGES, and R.-D. NEEF, "Models and Codes for the Nuclear Assessment of the ESS Target System," *Proc. 2nd Int. Topl. Mtg. Nuclear Applications of Accelerator Technology (AccApp'98)*, Gatlinburg, Tennessee, September 20–23, 1998, p. 22, American Nuclear Society (1998).

18. Information on ICANS is available on the Internet (http://www.pna.anl.gov/icans/icansdescript.html).

19. D. FILGES et al., ESS 94-4-T, European Spallation Neutron Source (Nov. 1994).

20. D. FILGES, R.-D. NEEF, and H. SCHAAL, "ICANS-XIII," *Proc. 13th Mtg. Int. Collaboration Advanced Neutron Sources*, PSI-Proc. 95-02, p. 537, Paul Scherrer Institute (Nov. 1995).

21. J. BELL, "ORIGEN," ORNL-4628, Oak Ridge National Laboratory (1973).

22. A. YU. KONOBEYEV et al., *J. Nucl. Mater.*, **195**, 286 (1992).

23. W. W. ENGLE, ORNL-K-1693, Oak Ridge National Laboratory (1967).

24. T. W. ARMSTRONG, "CASL—A Computer Aided Shielding Layout Code," (1985) (unpublished).

25. B. WOLFERTZ, "Entwicklung eines ingenieurmäßigen Simulationssystems zur Berechnung von Strahlenschutzparametern an Protonenbeschleunigern im Energiebereich bis 3 GeV," Dissertation, D 468, Wuppertal University (1995).

26. W. B. WILSON, "Nuclear Data Development and Shield Design for Neutrons Below 60 MeV," LA-7159-T, Los Alamos National Laboratory (1978).

27. R. G. ALSMILLER, Jr. and J. BARISH, "HILO, 66 Neutron, 21 Gamma Ray Group Cross Sections for Radiation Transport for Neutron Energies up to 400 MeV," ORNL/TM-7818, Oak Ridge National Laboratory (1981); see also ORNL-RSIC-DLC-87, Oak Ridge National Laboratory (1982); see also

"Neutron-Photon Multigroup Cross Sections for Neutron Energies ≤400-MeV," *Nucl. Sci. Eng.*, **80**, 448 (1982).

28. H. SCHAAL and D. FILGES, "Combination of the High Energy Libraries LANL and HILO as LAHI-Library for Deep Penetration Calculations," SNQ3J/BH120783, KFA Interne Aktennotiz, Kernforschungsanlage Juelich (1983); see also "RSIC Newsletter" DLC-128/LAHIMACK in RSIC Data Library Collection, Oak Ridge National Laboratory (June 1987).

29. J. MOLL, Juel-2435, Kernforschungsanlage Juelich (1991).

30. "Radiation Protection, Data for Use in Protection Against External Radiation," ICRP-51, International Commission on Radiological Protection (Mar. 1987).

31. P. CLOTH et al., *Proc. Specialists Mtg.*, Issy-les-Moulineaux, France, 1994, p. 219 (1994).

32. M. M. MEIER, C. A. GOULDING, G. L. MORGAN, and J. L. ULLMAN, "Neutron Yields from Stopping- and Near-Stopping-Length Targets for 256-MeV Protons," *Nucl. Sci. Eng.*, **104**, 339 (1990); see also M. M. MEIER, W. B. AMIAN, C. A. GOULDING, G. L. MORGAN, and C. E. MOSS, "Differential Neutron Production Cross Sections for 256-MeV Protons," *Nucl. Sci. Eng.*, **110**, 289 (1992).

33. T. NAKAMATO et al., "ICANS-XII," *Proc. 12th Mtg. Int. Collaboration Advanced Neutron Sources*, RAL-Proc. 94-025, p. T-80, Rutherford Appleton Laboratory, United Kingdom (1993).

34. S. MEIGO et al., "ICANS-XIII," *Proc. 13th Mtg. Int. Collaboration Advanced Neutron Sources*, PSI Proc. 95-02, p. 442 (1995).

35. S. LERAY, *Proc. Specialists Mtg.*, Issy-les-Moulineaux, France, 1994, p. 379 (1994); also presented at 2nd Int. Conf. on Accelerator-Driven Transmutation Technology, Kalmar, Sweden, June 3–7, 1996.

36. R. MICHEL et al., *Nucl. Instrum. Methods, B*, **103**, 183 (1995).

37. J. S. FRASER et al., *Can. J. Phys.*, **49**, 2061 (1971).

38. R. G. VASSILKOV and V. S. YUREVICH, "ICAN-XI," *Proc. 11th Mtg. Int. Collaboration Advanced Neutron Sources*, KEK 90-25, p. 340, National Laboratory for High-Energy Physics, Japan (1991).

39. G. MORGAN et al., *AIP Conf. Proc.*, **346**, 663 (1995).

40. M. S. ZUCKER et al., presented at 2nd Int. Conf. on Accelerator-Driven Transmutation Technology, Kalmar, Sweden, June 3–7, 1996.

41. J. FRÉHAUT, *AIP Conf. Proc.*, **346**, 673 (1995).

42. D. HILSCHER et al., presented at Int. Workshop on Nuclear Methods for Transmutation of Nuclear Waste: Problems, Perspectives, Cooperative Research, Dubna, Russia, May 29–31, 1996.

43. U. JAHNKE et al., "Experiment Proposal at COSY," COSY Program Advisory Committee, (Oct. 1995) (unpublished).

44. B. ANDERS et al., *Nucl. Instrum. Methods, A*, **277**, 56 (1989).

45. F. BARREIRO et al., *Nucl. Instrum. Methods, A*, **292**, 259 (1990).

46. R.-D. NEEF, "Radiation Physics Experiments to Develop the Target-Moderator-Reflector System for ESS," ANL-98/33, Vol. II, p. 44, Argonne National Laboratory (1998).

Detlef Filges [Diploma, physics, University of Mainz, Germany, 1969; Dr rer nat, nuclear engineering, Rheinisch-Westfaelische Technische Hochschule (RWTH) -Aachen, Germany, 1976] is a professor at Bergische University Wuppertal, Germany, and a senior scientist and group leader at the Forschungszentrum Juelich (FZJ) Institut fuer Kernphysik (IKP). Currently, he is the supervisor for the nuclear layout of the target station of the European Nuclear Spallation Source (ESS). His background includes detector development in medium- and high-energy physics, particle transport and particle interaction with matter, spallation physics, accelerator applications, and reactor physics.

Ralf D. Neef (Diploma, physics, 1968, and Dr rer nat, nuclear engineering, 1976, RWTH-Aachen, Germany) is a senior scientist at IKP at FZJ. His background includes high-temperature gas cooled reactor (HTGR) core physics and design, and he is currently working on the ESS project in the areas of target-moderator-reflector design, and spallation and neutron physics.

Hartwig Schaal (Diploma, physics, 1973, and Dr-Ing, nuclear engineering, 1981, University of Stuttgart, Germany) is a senior scientist at IKP at FZJ. His background includes analysis and interpretation of critical experiments for HTGRs, design of high-energy electromagnetic shower detectors, and spallation physics. He is currently working on deep penetration and radioactivity problems for spallation neutron sources.